JOURNAL OF GUIDANCE, CONTROL, AND DYNAMICS
Vol. 20, No. 2, March–April 1997

Pole-Placement Technique for Magnetic Momentum Removal of Earth-Pointing Spacecraft

Hari B. Hablani*
Rockwell International Corporation, Downey, California 90241-7009

A linear pole-placement technique is presented for magnetic momentum removal of Earth-pointing spacecraft. First probed are the two most commonly used momentum removal schemes, linear and bang-bang $\boldsymbol{H} \times \boldsymbol{B}$ schemes (where $\boldsymbol{H}$ is the excess angular momentum vector and $\boldsymbol{B}$ is the geomagnetic field vector), both based on a comparison between a constant disturbance torque and an averaged magnetic control torque acting on a spacecraft. Through analysis and illustrations, it is shown that these two methods lack a precise technique for determining control gains or strength (in ampere meter squared) of roll, pitch, and yaw electromagnets. As an alternative, a linear, closed-loop, pole-placement technique is devised, which correlates control gains with the closed-loop pole locations and steady-state amplitudes of roll/yaw and pitch momentum under an orbit-averaged magnetic controller and disturbances. Special cases of low- and high-inclination orbits where pitch and yaw electromagnets, respectively, are ineffective are formulated. This new scheme and the mentioned two classical schemes of momentum removal are compared and illustrated, and generally applicable conclusions are drawn.

I. Introduction

DEPENDING on spacecraft mission and constraints, momentum management of spacecraft has been orchestrated in the past in many different ways. For example, momentum removal of control moment gyros of Skylab, an inertially stabilized forerunner of this decade's space station, was effected using gravity gradient torque generated by special attitude maneuvers.[1,2] The momentum management of the forthcoming Earth-pointing space station is designed analogously, seeking an attitude offset from the local vertical such that the resulting gravity gradient torque is in equilibrium with the disturbing atmospheric torque.[3–8] Because the torque-equilibrium attitude of the space station is tracked by the same controller that manages its momentum, the momentum management and attitude control, in Refs. 3–8, are both designed together. Mathematical apparatus for pole placement using linear quadratic regulator,[3,4] digital control,[5,6] and μ synthesis[7] of modern control theory have been applied to design momentum dumping. In this context, the classical control technique of relating gains with the desired closed-loop pole locations[8] has also been applied. Sometimes, however, the special attitude maneuvers required in these designs conflict with the spacecraft mission. Magnetic torquing, then, has been frequently used for momentum removal in lieu of gravity gradient torque: Earth-pointing global positioning system (GPS) satellites,[9,10] sun-pointing Solar Maximum Mission,[11] inertially stabilized Gamma Ray Observatory,[12] for example. Magnetic momentum removal has been practiced for nearly three decades[13,14] but, insofar as we are aware of, its design using pole-placement technique has not been formulated although, surprisingly, as we shall see, doing so is much simpler than designing momentum removal by gravity gradient torque. In the latter case, the attitude control and momentum management must be designed together, rendering the analysis less amenable, whereas in the former case, the two problems are considered separately. This separate consideration is justified because the spacecraft attitude near its nominal orientation is controlled with momentum storage devices operating at a bandwidth 10 times or more wider than the bandwidth of the magnetic momentum removal controller.[15] It is this simpler problem that is considered in this paper.

Ideally, the momentum storage devices, say, reaction wheels, should counteract the cyclic (in the inertial frame) environmental torques, and the electromagnets should counteract the secular disturbances. However, if the momentum removal controller is not designed appropriately, the reaction wheels would oppose secular disturbances as well, imposing a periodic removal of a larger accumulated momentum. This, in turn, increases power consumption and electric losses of the wheels, usurps their torque and momentum capacity to absorb nonenvironmental torques such as one from articulated sensors, and mandates the selection of wheels and magnets of higher capacity and cost. Camillo and Markley[11] analyzed linear and bang-bang $\boldsymbol{H} \times \boldsymbol{B}$ (where $\boldsymbol{H}$ is the excess angular momentum vector and $\boldsymbol{B}$ is the geomagnetic field vector) magnetic controllers, and they conceived a control effectiveness ratio between the orbit-averaged magnetic control torque and the opposite secular disturbance torque. (Such a ratio was informally introduced earlier in Ref. 14.) The electromagnets are sized to render this ratio greater than unity for the satellite's entire lifetime. But the ratio is governed by the strength of the roll, pitch, and yaw electromagnets or by their linear gains, and Ref. 11 does not offer a technique for selecting them individually. Indeed, a standard assumption in many previous works has been that the three capacities or the three linear gains are all equal. There seems to be no technique in the literature, except Ref. 16, relating the gains of the electromagnets with the steady-state, residual roll/yaw and pitch momentum components of a cylindrical momentum envelope or with the closed-loop poles of the magnetic momentum removal controller. Even the exception, Ref. 16, is limited to only one electromagnet in the geosynchronous orbit (roll/yaw) plane.

In contrast, this paper presents a closed-loop pole-placement technique for Earth-pointing spacecraft in a general circular orbit, outfitted with three electromagnets, one along each axis. This brings us to the contents. The text consists of three parts. The first two parts deal with the orbit-averaged static analysis of linear and bang-bang $\boldsymbol{H} \times \boldsymbol{B}$ control laws, following Ref. 11. These techniques are called static because they are based on the control effectiveness ratio, not on eigenanalysis of the controller's performance. The techniques are illustrated for an Earth-pointing spacecraft with sun-tracking arrays under environmental torques about all three axes; the strong and weak points of the techniques are brought out. The third part formulates a novel, linear, orbit-averaged magnetic controller, alluded to earlier, based on pole placement. The use of linear quadratic regulator theory to relate weighting matrices with the closed-loop poles, as in Refs. 3–6, is not required, for a straightforward determination of closed-loop eigenvalues, and their relationship with steady-state momentum amplitudes about each of the three axes, after Lebsock,[16] seems adequate and elegant at once. The special cases of low- and high-inclination orbits are considered. Numerical results are presented illustrating the ease and simplicity of the

Received March 16, 1995; revision received Nov. 12, 1996; accepted for publication Nov. 27, 1996.

*Principal Engineering Specialist, Space Systems Division, 12214 Lakewood Boulevard. Associate Fellow AIAA.

technique with which specified steady-state momentum amplitudes, according to desired wheel size, result in closed-loop pole locations and electromagnets size.

II. Orbit-Averaged Magnetic Momentum Removal Control Laws

Linear Controller: Static Analysis

According to $\boldsymbol{H} \times \boldsymbol{B}$ law, the magnetic dipole vector $\boldsymbol{M}$ is varied; thus

$$\boldsymbol{M} = g_1[(\boldsymbol{H} \times \boldsymbol{B}) \bullet \boldsymbol{b}_1]\boldsymbol{b}_1 + g_2[(\boldsymbol{H} \times \boldsymbol{B}) \bullet \boldsymbol{b}_2]\boldsymbol{b}_2 + g_3[(\boldsymbol{H} \times \boldsymbol{B}) \bullet \boldsymbol{b}_3]\boldsymbol{b}_3 \tag{1}$$

[see Ref. 11, Eq. (4.b)], where g_1, g_2, and g_3 are the positive gains of roll, pitch, and yaw electromagnets, respectively, and $\boldsymbol{b}_1$, $\boldsymbol{b}_2$, and $\boldsymbol{b}_3$ are unit vectors along these spacecraft-fixed axes. It is known that a component of the magnet $\boldsymbol{M}$ parallel to the geomagnetic field $\boldsymbol{B}$ would not produce a torque. Yet, by introducing three independent gains, g_1, g_2, and g_3 in Eq. (1), $\boldsymbol{M}$ is allowed to be independent of $\boldsymbol{B}$. This is still helpful because the spacecraft orbit considered here is general, and the three independent gains will enable the designer to orient $\boldsymbol{M}$ suitably, according to the orbit-averaged magnetic field and spacecraft orbit geometry. Because the excess angular momentum $\boldsymbol{H}$ in Eq. (1) is essentially due to a constant (in an inertial frame) external disturbance torque $\boldsymbol{\Gamma}$, one can write[11]

$$\boldsymbol{H} = H\hat{\boldsymbol{H}} = H\hat{\boldsymbol{\Gamma}} \tag{2}$$

where $H = |\boldsymbol{H}|$, and $\hat{\boldsymbol{H}}$ and $\hat{\boldsymbol{\Gamma}}$ are parallel unit vectors along parallel vectors $\boldsymbol{H}$ and $\boldsymbol{\Gamma}$. For an Earth-pointing spacecraft with a sun-tracking array, the spacecraft that led to this study, the solar radiation and gravity gradient torques were found to be major external disturbances. With the solar array on the orbit normal side, denoted $-y_c$ side of the orbit (c for circular orbit), the corresponding constant torque $\boldsymbol{\Gamma}$ in the standard inertial frame $\mathcal{F}^{\ell bn}$ has the form

$$-y_c \text{ array: } \boldsymbol{\Gamma}^{\mathcal{F}^{\ell bn}} = \begin{bmatrix} -G_a c\theta_0 \\ G_a s\theta_0 \\ -g_{b,g} \end{bmatrix}$$
$$|\boldsymbol{\Gamma}| = \left(G_a^2 + g_{b,g}^2\right)^{\frac{1}{2}} \triangleq \Gamma \tag{3}$$

(see Sec. III), where the frame $\mathcal{F}^{\ell bn}$ consists of a unit vector $\boldsymbol{\ell}$ along the ascending node line, a unit vector $\boldsymbol{n}$ normal to the spacecraft orbit plane, and $\boldsymbol{b}$ completing the right-handed triad. In Eq. (3), G_a is the amplitude of a resultant torque in the orbit plane arising from gravity gradient and solar radiation and $g_{b,g}$ is a bias gravity gradient torque about the nominal pitch axis y_c opposite to $\boldsymbol{n}$. The angle θ_0 defines the initial orientation of the solar array normal to sun rays,[17] and $s\cdot = \sin(\cdot)$, $c\cdot = \cos(\cdot)$. For comparison, note that the orbit-averaged disturbance torque acting on the Earth-pointing satellite in Ref. 11 has a pitch component only, but the torque in this study has all three components. Returning to Eq. (3), we note that the parallel unit vectors $\hat{\boldsymbol{H}}$ and $\hat{\boldsymbol{\Gamma}}$ can be determined from this equation. It can be shown that the component of the magnetic control torque $\boldsymbol{N}_c = \boldsymbol{M} \times \boldsymbol{B}$ along the unit vector $\hat{\boldsymbol{\Gamma}}$ is

$$\boldsymbol{N}_c \bullet \hat{\boldsymbol{\Gamma}} = -H\left[g_1(\boldsymbol{V}_x \bullet \boldsymbol{B})^2 + g_2(\boldsymbol{V}_y \bullet \boldsymbol{B})^2 + g_3(\boldsymbol{V}_z \bullet \boldsymbol{B})^2\right] \tag{4}$$

[see Eq. (7b), Ref. 11], where the vectors $\boldsymbol{V}_x$, $\boldsymbol{V}_y$, $\boldsymbol{V}_z$ are given by

$$\boldsymbol{V}_x = \hat{\boldsymbol{\Gamma}} \times \boldsymbol{b}_1 \qquad \boldsymbol{V}_y = \hat{\boldsymbol{\Gamma}} \times \boldsymbol{b}_2 \qquad \boldsymbol{V}_z = \hat{\boldsymbol{\Gamma}} \times \boldsymbol{b}_3 \tag{5}$$

[Ref. 11, Eq. (8)] with $\boldsymbol{b}_1$, $\boldsymbol{b}_2$, and $\boldsymbol{b}_3$ being the spacecraft-fixed unit vectors along roll, pitch, and yaw axes, respectively. It is evident from Eq. (4) that, for positive g_1, g_2, g_3 gains, the control torque $\boldsymbol{N}_c \bullet \hat{\boldsymbol{\Gamma}}$ opposes the excess momentum H, as desired. Because the roll and yaw unit vectors $\boldsymbol{b}_1$ and $\boldsymbol{b}_3$ rotate in an inertial frame, the vectors $\boldsymbol{V}_x$, $\boldsymbol{V}_y$, $\boldsymbol{V}_z$ are time varying. Further, since the disturbance torque $\boldsymbol{\Gamma}$ is constant in the inertial frame $\mathcal{F}^{\ell bn}$ over a few orbits, it is desirable to know the average, constant value of the control torque $\boldsymbol{N}_c \bullet \hat{\boldsymbol{\Gamma}}$ denoted $\langle \boldsymbol{N}_c \bullet \hat{\boldsymbol{\Gamma}} \rangle$. To calculate this, we note that in the local-vertical–local-horizontal orbit frame $\mathcal{F}^c$ and in the inertial frame $\mathcal{F}^{\ell bn}$ the tilted dipole geomagnetic field model is expressed, respectively, as[18]

$$\boldsymbol{B}^{\mathcal{F}^c} = \kappa \begin{bmatrix} s\xi c(\omega_0 t - \eta) \\ -c\xi \\ 2s\xi s(\omega_0 t - \eta) \end{bmatrix}$$
$$\boldsymbol{B}^{\mathcal{F}^{\ell bn}} = \kappa \begin{bmatrix} \frac{1}{2}s\xi\{s\eta - 3s(2\omega_0 t - \eta)\} \\ \frac{1}{2}s\xi\{-c\eta + 3c(2\omega_0 t - \eta)\} \\ c\xi \end{bmatrix} \tag{6}$$

where $\kappa = \mu_m / r^3$; μ_m is the Earth's dipole strength; r is the radius of the circular orbit; ξ is the instantaneous inclination of the spacecraft orbit with the geomagnetic equator; η is the angle from the ascending node of the orbit relative to the Earth's equator to the ascending node of the orbit relative to the geomagnetic equator[13]; ω_0 is the orbit rate; and t is the time. Denoting the spacecraft orbit inclination as i and the geomagnetic dipole tilt as γ, the angle ξ oscillates between $i - \gamma$ and $i + \gamma$ in one day, due to the Earth's rotation. Furthermore, the tilted dipole model of the geomagnetic field is used here because it is analytically simple and, in the context of GPS satellites, it was found to represent most closely the real, in-flight magnetic momentum removal performance.[19] As a result of a tight attitude control loop (not considered here), the spacecraft frame $\mathcal{F}^b$: $\boldsymbol{b}_1\boldsymbol{b}_2\boldsymbol{b}_3$ is assumed to be aligned with the orbit frame $\mathcal{F}^c$. Therefore, transforming $\hat{\boldsymbol{\Gamma}}$ from Eq. (3) to the orbit frame $\mathcal{F}^c$, substituting that in Eq. (5) and then in Eq. (4) and employing $\boldsymbol{B}^{\mathcal{F}^c}$ from Eq. (6), the following orbit-averaged values of the square terms in Eq. (4) are arrived at:

$$\rho_x \triangleq \left\langle (\boldsymbol{V}_x \bullet \boldsymbol{B})^2 \right\rangle = \kappa^2\left[\tfrac{1}{2}(\hat{G}_a c\xi)^2 + 2(\hat{g}_{b,g} s\xi)^2 - \hat{G}_a \hat{g}_{b,g} s2\xi s(\eta + \theta_0)\right] \tag{7a}$$

$$\rho_y \triangleq \left\langle (\boldsymbol{V}_y \bullet \boldsymbol{B})^2 \right\rangle = \kappa^2\left(\tfrac{1}{2}\hat{G}_a s\xi\right)^2\left[\tfrac{9}{2} + \cos^2(\eta + \theta_0)\right] \tag{7b}$$

$$\rho_z \triangleq \left\langle (\boldsymbol{V}_z \bullet \boldsymbol{B})^2 \right\rangle = \tfrac{1}{2}\kappa^2\left[(\hat{G}_a c\xi)^2 + (\hat{g}_{b,g} s\xi)^2 + \hat{G}_a \hat{g}_{b,g} s2\xi s(\eta + \theta_0)\right] \tag{7c}$$

where $\langle \bullet \rangle$ denotes a quantity averaged over one orbit, $s2\xi = \sin(2\xi)$, and

$$\hat{G}_a = G_a / \Gamma \tag{8}$$

$$\hat{g}_{b,g} = g_{b,g} / \Gamma \tag{9}$$

It is reassuring that, for the orbit plane torque amplitude G_a equal to zero, Eq. (7) and therefore Eq. (4) specialize to Eq. (20) of Ref. 11. Next, to facilitate a reasonable selection of the gains in Eq. (4), we observe that, when the average values [Eq. (7)] are placed in Eq. (4), the cross-product terms $\hat{G}_a \hat{g}_{b,g}$ cancel each other if we set $g_3 = 2g_1$. We, therefore, adopt this intuitive relationship. Moreover, let $g_2 = \chi_g g_1$, where $\chi_g > 0$. Substituting Eqs. (7) in Eq. (4) and dividing the equation by the magnitude Γ, we arrive at the control effectiveness ratio R_L (L for linear controller) involving the factor H/Γ. By definition, the majority of the momentum $\boldsymbol{H}$ is caused by the constant disturbance torque [Eq. (3)]; assuming that the momentum accumulated in one orbit period must be removed within one orbit, one has $H/\Gamma = \tau_0 =$ orbit period. Moreover, since the ratio R_L must be greater than unity, the unknown gain g_1 must obey the condition

$$g_1 \geq \left(\kappa^2\tau_0\right)^{-1}\left[\hat{G}_a^2\left\{\tfrac{3}{2}c^2\xi + \tfrac{1}{4}\chi_g s^2\xi\left[\left(\tfrac{9}{2} + \cos^2\overline{\eta + \theta_0}\right)\right]\right\} + 3\hat{g}_{b,g}^2 s^2\xi\right]^{-1} \tag{10}$$

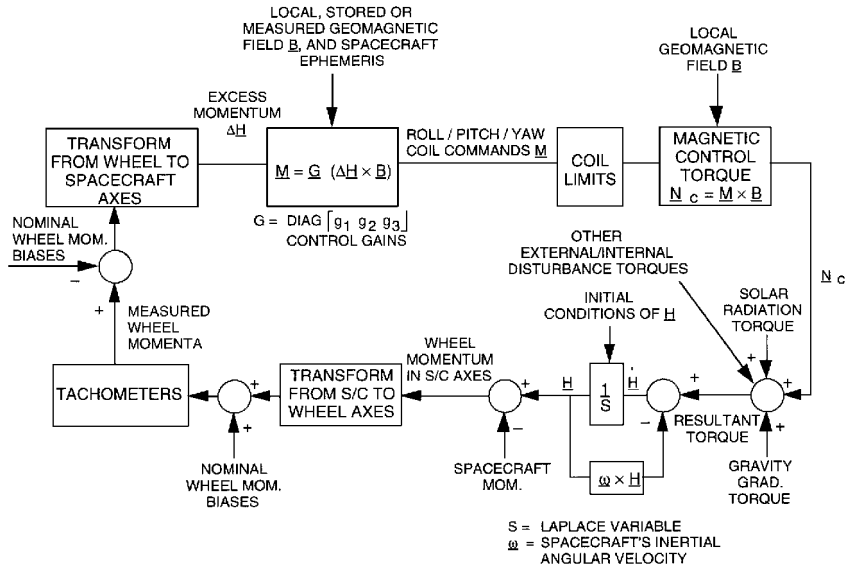

Fig. 1 Linear magnetic momentum removal controller.

where $s^2\cdot = \sin^2(\cdot)$ and $c^2\cdot = \cos^2(\cdot)$. For $\chi_g = 4$, and because $\hat{G}_a^2 + \hat{g}_{b,g}^2 = 1$, Eq. (10) simplifies to

$$g_1 \geq \left(\kappa^2\tau_0\right)^{-1}\left[\hat{G}_a^2\left\{\tfrac{3}{2} + s^2\xi c^2(\eta+\theta_0)\right\} + 3s^2\xi\right]^{-1} \qquad (11)$$

Finally, if the right-hand side of the condition (10) is denoted $g_{1,\min}$, the three gains will be

$$g_1 \geq g_{1,\min} \qquad g_2 = \chi_g g_1 \qquad g_3 = 2g_1 \qquad (12)$$

A shortcoming of the technique is now evident: it does not clearly state what the gains should be, except that $g_1 \geq g_{1,\min}$.

Figure 1 depicts the preceding linear magnetic momentum removal controller in a block diagram form. Here $\boldsymbol{H}$ is the total, instantaneous angular momentum of the spacecraft and wheels, expressed in the spacecraft frame. The excess angular momentum used in the preceding analysis is obtained by subtracting the spacecraft's own momentum from $\boldsymbol{H}$. But, because of the assumed tight attitude control, the spacecraft's own momentum would be due only to its once-per-orbit rotation about the pitch axis, ignored in the analysis for simplicity but accommodated in the simulation as shown in the figure. The reaction wheels, the momentum storage device considered, are arranged in a pyramid configuration of four wheels and nominally rotate at bias speeds, with zero net momentum in the spacecraft frame. Wheel tachometers measure the instantaneous speeds, from which the excess momentum $\Delta\boldsymbol{H}$ (denoted $\boldsymbol{H}$ earlier) is calculated by calling upon the transformation matrices. The desired magnetic dipole vector $\boldsymbol{M}$ is then determined according to Eq. (1), employing the magnetometers' reading of the local geomagnetic field $\boldsymbol{B}$ or its stored value at the current location of the spacecraft in the orbit. Interacting with the local field, the electromagnets then produce a magnetic control torque $\boldsymbol{N}_c$ for momentum removal.

Illustration

This illustration and those following pertain to an Earth-pointing spacecraft with a sun-tracking solar array in a 116-min orbit inclined at 28.5 deg. The annual variation of the corresponding components $\hat{G}_a$ and $\hat{g}_{b,g}$ of the unit vector $\hat{\boldsymbol{\Gamma}}$ is shown in Fig. 2. This variation is based on zero and π-rad yaw orientations of the spacecraft, as required for sun-tracking over one year. Also, the variation of G_a and $g_{b,g}$ stems from the varying orientation of the solar array for tracking the sun, causing the products of inertia of the spacecraft to vary continuously. It is clear from Fig. 2 that the roll/yaw torque amplitude G_a predominates over the pitch bias torque $g_{b,g}$, for $\hat{G}_a = -0.95$ on the average. Because it is not adequate merely to have the gain $g_1 = g_{1,\min}$, we set $g_1 = 8g_{1,\min}$, the factor 8 selected through simulation experiments for a satisfactory performance of the controller. Using $\chi_g = 4$, and $\hat{G}_a$, $\hat{g}_{b,g}$ shown in Fig. 2, the

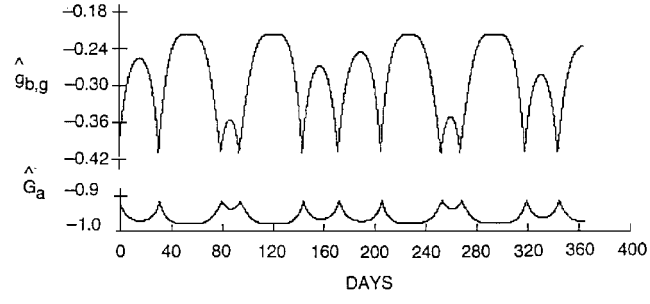

Fig. 2 Annual variation of the components G_a and $g_{b,g}$ of the unit vector $\hat{\Gamma}$.

control gain g_1 is obtained from Eq. (11). Because of the Earth's spinning and the orbital nodal regression of 4.18 deg/day in this example, the inclination angle ξ oscillates between $i+\gamma$ and $i-\gamma$ in a day and causes daily variations in the gain g_1. In addition, the nearly monthly variations in $\hat{G}_a$ and $\hat{g}_{b,g}$ shown in Fig. 2 cause further periodic changes in g_1. In reality, of course, $\hat{G}_a$ and $\hat{g}_{b,g}$ are not known exactly.

Figure 3 illustrates steady-state wheel momentum expressed in the local-vertical–local-horizontal orbit frame $\mathcal{F}^c$ under gravity gradient and solar radiation torque and magnetic control torque. The performance shown is for 50 orbits (4.03 days, with the orbit period $\tau_0 = 6959$ s). The magnets are turned on when the wheel momentum about any axis exceeds a threshold momentum equal to the cyclic momentum amplitude about that axis (stated in Fig. 3). This feature is not shown in the block diagram (Fig. 1) because, subsequently, it is deleted from the controller; otherwise the cyclic momentum amplitude must be estimated in orbit. Also, the cyclic momentum is usually much smaller than the accumulated momentum to be removed; for example, presently, the momentum buildup in one orbit in roll/yaw axes is $1.18\ \mathrm{N\cdot m\cdot s}$ and in pitch $0.26\ \mathrm{N\cdot m\cdot s}$ compared to the cyclic amplitude quoted in Fig. 3. It is, therefore, safe to ignore the cyclic momentum. The roll, pitch, yaw dipole strengths vary over 55 orbits as shown in Fig. 4, oscillating at orbit frequency ω_0 and its multiples and at 24-h period frequency.

Bang-Bang Controller: Static Analysis

For this controller, the electromagnets are either fully on with + or − polarity or off, the polarity selected according to the $\boldsymbol{H}\times\boldsymbol{B}$ law[11]

$$M_i = C_i\ \mathrm{sgn}(\boldsymbol{H}\times\boldsymbol{B})_i \qquad (i = x, y, z) \qquad (13)$$

where C_i is the maximum strength of the electromagnet along the i axis. Although this scheme is closed loop and autonomous, an open-loop ground-controlled bang-bang scheme is in use instead

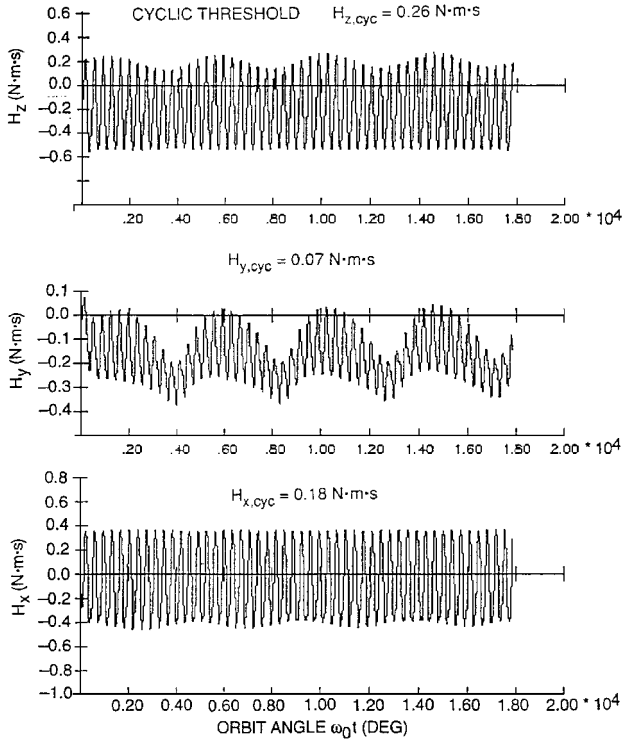

Fig. 3 Wheel momentum expressed in local-vertical–local-horizontal orbit frame.

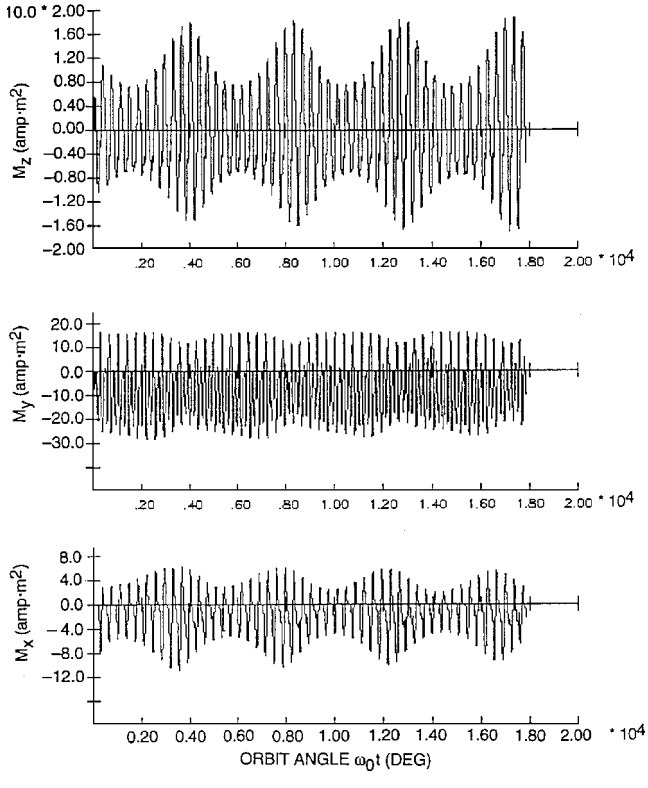

Fig. 4 Variation of electromagnets' strengths along roll, pitch, and yaw axes parallel to the local-vertical–local-horizontal orbit frame.

for the GPS satellites,[9,10] with the switching times governed by the satellite visibility from the ground station. Also, the discrete level of the dipole could be different in different segments of the orbit for maximum utilization of the magnetic field, in accordance with a cell mapping approach in Ref. 20. The orbit-averaged component of the control torque $\boldsymbol{N}_c$ along the disturbance torque unit vector $\hat{\boldsymbol{\Gamma}}$ is[11]

$$k_B \triangleq \langle|\boldsymbol{N}_c \bullet \hat{\boldsymbol{\Gamma}}|\rangle = C_x\langle|\boldsymbol{V}_x \bullet \boldsymbol{B}|\rangle + C_y\langle|\boldsymbol{V}_y \bullet \boldsymbol{B}|\rangle + C_z\langle|\boldsymbol{V}_z \bullet \boldsymbol{B}|\rangle \quad (14)$$

For $\boldsymbol{\Gamma}$ defined by Eq. (3), it can be shown that orbit-averaged values of $|\boldsymbol{V}_x \bullet \boldsymbol{B}|$ and $|\boldsymbol{V}_z \bullet \boldsymbol{B}|$ are

$$\langle|\boldsymbol{V}_i \bullet \boldsymbol{B}|\rangle = 2\kappa A_i/\pi \qquad (i = x, z) \quad (15)$$

where the amplitudes A_x and A_z, defined in terms of the quantities ρ_x, ρ_y, ρ_z [Eqs. (7)], are

$$A_i^2 = 2\rho_i \big/ \kappa^2 \qquad (i = x, z) \quad (16)$$

Evaluation of the orbit-averaged quantity $\langle|\boldsymbol{V}_y \bullet \boldsymbol{B}|\rangle$ is tricky, however, due to the bias term $\cos(\eta + \theta_0)$ in $(\boldsymbol{V}_y \bullet \boldsymbol{B})$. Using the formulaton of quasiquarter-orbit switching true anomalies in Ref. 18, it can be shown that

$$\langle|\boldsymbol{V}_y \bullet \boldsymbol{B}|\rangle = \kappa|\hat{G}_a \sin\xi||6\sin 2\theta_1 + (\pi - 4\theta_1)\cos(\eta + \theta_0)|/2\pi \quad (17)$$

where the orbit angle θ_1 is

$$\theta_1 \triangleq \tfrac{1}{2}\cos^{-1}\left[\tfrac{1}{3}\cos(\eta + \theta_0)\right] \quad (18)$$

After reconciling the notations and using the definition of θ_1, Eq. (17) agrees with Eq. (11) of Ref. 11, where, in this application, the coefficient B (not related with the field $\boldsymbol{B}$) is zero. Substituting Eqs. (15) and (17) in Eq. (14), we finally arrive at

$$k_B = 2\kappa(C_x A_x + C_z A_z)/\pi + \kappa C_y|\hat{G}_a s\xi|6s2\theta_1 + (\pi - 4\theta_1)c(\eta + \theta_0)|/2\pi \quad (19)$$

and the control effectiveness ratio R_B is found from $R_B = k_B/\Gamma \geq 1$. Just as with the linear gains, the limitation of this bang-bang control approach is that it is not clear how the electromagnet strengths C_x, C_y, and C_z are to be chosen. The extrema of the amplitudes A_x and A_z suggest $C_z = 2C_x$ (in line with the earlier $g_3 = 2g_1$ relationship), and $C_y = C_x \cot i$. With these special ratios, the minimum value of C_x (in ampere meter squared) is determined from the condition that the ratio R_B must be greater than unity.

Illustration

For the spacecraft used in the previous illustration and with $C_x = 10$, $C_y = 18.4$, and $C_z = 20$, Fig. 5 shows a momentum removal performance of the bang-bang controller. The associated ratio R_B varies throughout the year, with minimum 2.4 and maximum 7. Comparing the spacecraft momentum in Fig. 5 with that in Fig. 3, it is evident that the bang-bang controller controls the momentum and thereby the wheel speeds about the cyclic thresholds more tightly than the linear controller does for the gains selected. The polarity reversal of the roll electromagnet is shown in Fig. 6; the pitch and yaw electromagnets vary likewise. The strengths of the electromagnets are generally larger than the time-varying strengths in Fig. 4. The variation of the magnetic control torque (N_x, N_y, N_z) about the three axes is depicted in Fig. 7, wherein daily oscillations caused by the Earth's spinning are apparent. Because the magnets are fully on all of the time, they consume more power than the linear controller does. The tighter momentum control exhibited in Fig. 6 is attributed to this higher power consumption and to the frenetic pace at which the magnets change their polarity.

Linear Controller: Pole Placement Technique

The electromagnet vector $\boldsymbol{M}$ is still governed by Eq. (1), which, in the orbit frame $\mathcal{F}^c$, appears as

$$\boldsymbol{M} = \boldsymbol{c}_1 g_1(H_y B_z - H_z B_y) + \boldsymbol{c}_2 g_2(H_z B_x - H_x B_z) + \boldsymbol{c}_3 g_3(H_x B_y - H_y B_x) \quad (20)$$

where the unit vector triad $\boldsymbol{c}_1, \boldsymbol{c}_2, \boldsymbol{c}_3$ is along the local-vertical–local-horizontal orbit frame $\mathcal{F}^c$; H_x, H_y, and H_z are the excess momenta and B_x, B_y, and B_z are the geomagnetic field components, both in $\mathcal{F}^c$ along the x, y, and z axes, respectively. The scalar form of the magnetic control torque $\boldsymbol{N}_c = \boldsymbol{M} \times \boldsymbol{B}$ in the orbit frame $\mathcal{F}^c$ is

$$\boldsymbol{N}_c = \boldsymbol{c}_1[g_2(H_z B_x - H_x B_z)B_z - g_3(H_x B_y - H_y B_x)B_y] + \boldsymbol{c}_2[g_3(H_x B_y - H_y B_x)B_x - g_1(H_y B_z - H_z B_y)B_z] + \boldsymbol{c}_3[g_1(H_y B_z - H_z B_y)B_y - g_2(H_z B_x - H_x B_z)B_x] \quad (21)$$

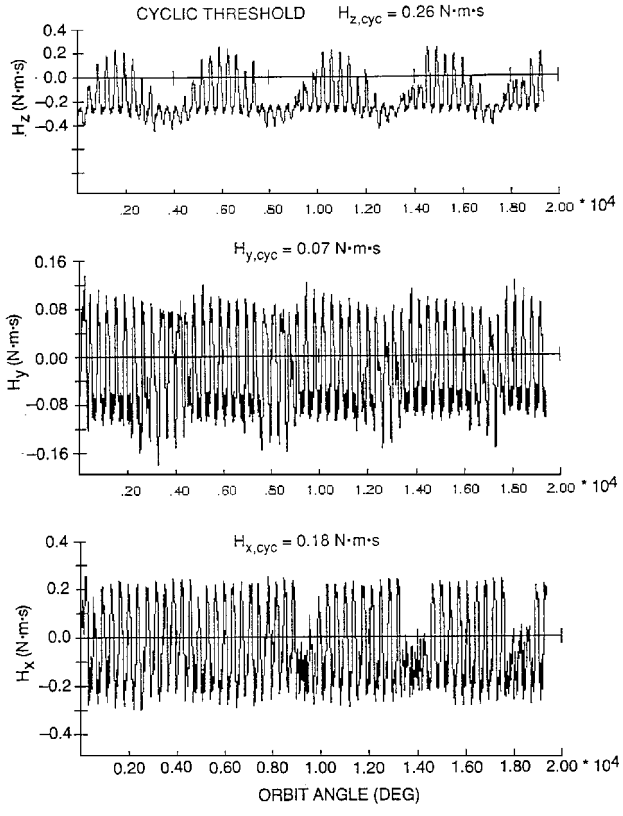

Fig. 5 Performance of a bang-bang magnetic controller: wheel momentum in local-vertical–local-horizontal orbit frame.

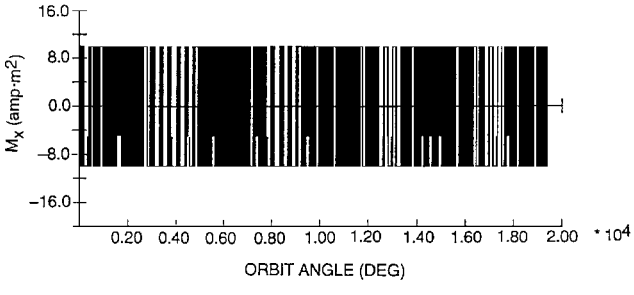

Fig. 6 Polarity reversal of the roll electromagnet for a bang-bang magnetic controller.

Because the magnetic field varies throughout the orbit, the influence of the control torque $\boldsymbol{N}_c$ on the momentum components H_x, H_y, and H_z is not readily amenable to analysis, although Carrington et al.[15] have attempted invoking linear quadratic regulator theory. It seems more enlightening, though, to use instead the following orbit averages in Eq. (21), using Eq. (6a):

$$\left\langle B_x^2 \right\rangle = \tfrac{1}{2}\kappa^2 \sin^2 \xi \qquad \left\langle B_y^2 \right\rangle = \kappa^2 \cos^2 \xi \qquad \left\langle B_z^2 \right\rangle = 2\kappa^2 \sin^2 \xi \tag{22}$$

$$\langle B_x B_y \rangle = 0 \qquad \langle B_y B_z \rangle = 0 \qquad \langle B_z B_x \rangle = 0 \tag{23}$$

which yield the following orbit-averaged control torque $\langle \boldsymbol{N}_c \rangle$:

$$\langle \boldsymbol{N}_c \rangle = -\boldsymbol{c}_1 \kappa^2 H_x \left[2g_2 s^2\xi + g_3 c^2 \xi \right] - \boldsymbol{c}_2 \kappa^2 H_y s^2 \xi (g_3/2 + 2g_1) - \boldsymbol{c}_3 \kappa^2 H_z \left[g_1 c^2 \xi + \tfrac{1}{2} g_2 s^2 \xi \right] \tag{24}$$

Equation (24) indicates that a roll dipole with a gain g_1 produces a pitch torque proportional to $2 \sin^2 \xi$ and a yaw torque proportional to $\cos^2 \xi$; likewise, the pitch and yaw dipoles. Additionally, for the roll and yaw electromagnets to be equally effective in producing a pitch torque, g_3 must be $4g_1$; similarly, the gains for the roll and pitch electromagnets must bear the ratio $g_2 = 2g_1 \cot^2 \xi$ to produce a yaw torque equally effectively. Viewed thus, the earlier intuitive

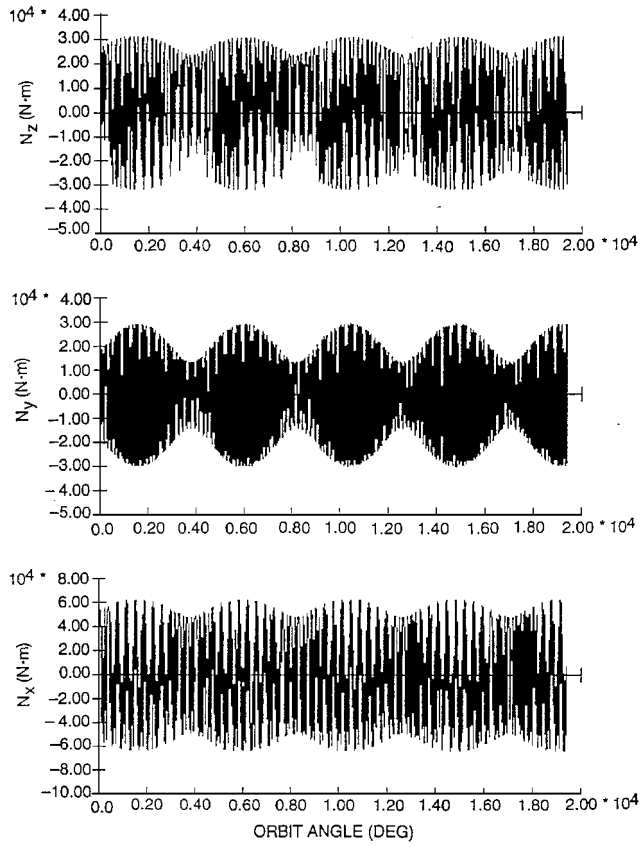

Fig. 7 Magnetic control torque about roll, pitch, and yaw axes.

relationships (12) and $C_z = 2C_x$, $C_y = C_x \cot i$ do not appeal now. Notice that the control torque exerted by each dipole depends on the orbit inclination through the angle ξ.

To conduct a closed-loop eigenanalysis of the linear controller, rewrite the right-hand side of Eq. (24) as

$$\langle \boldsymbol{N}_c \rangle = -\boldsymbol{c}_1 H_x \alpha_x - \boldsymbol{c}_2 H_y \alpha_y - \boldsymbol{c}_3 H_z \alpha_z \tag{25}$$

where

$$\alpha_x \triangleq \kappa^2 \left(2g_2 \sin^2 \xi + g_3 \cos^2 \xi \right) \tag{26a}$$

$$\alpha_y \triangleq \kappa^2 \sin^2 \xi (2g_1 + g_3/2) \tag{26b}$$

$$\alpha_z \triangleq \kappa^2 \left(g_1 \cos^2 \xi + \tfrac{1}{2} g_2 \sin^2 \xi \right) \tag{26c}$$

A typical Earth-pointing spacecraft's momentum components, expressed in the orbit frame, under the disturbance torque Eq. (3) and the control torque Eq. (25) are governed by

$$\dot{H}_x + \alpha_x H_x - \omega_0 H_z = G_a \sin(\omega_0 t + \theta_0) \tag{27a}$$

$$\dot{H}_y + \alpha_y H_y = g_{b,g} \tag{27b}$$

$$\dot{H}_z + \alpha_z H_z + \omega_0 H_x = G_a \cos(\omega_0 t + \theta_0) \tag{27c}$$

From the second-order characteristic equation associated with the roll/yaw momentum equations (27a) and (27c), the following necessary and sufficient conditions are derived: $\alpha_x + \alpha_z > 0$ and $\alpha_x \alpha_z + \omega_0^2 > 0$, which are satisfied easily by requiring that $\alpha_x > 0$ and $\alpha_z > 0$. The possibility that α_x or α_z could be negative and yet satisfy the former pair of conditions is ignored here. On the other hand, the uncoupled pitch momentum equation (27b) will be stable if $\alpha_y > 0$. Recalling the definitions (26), the stability conditions are met easily by requiring that the gains be all positive.

To arrive at the desired closed-loop pole locations, the steady-state roll/yaw momentum amplitudes, $H_{x,ss}$ and $H_{z,ss}$ respectively, are determined by solving Eqs. (27a) and (27c) together. To specify

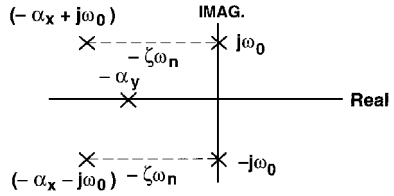

Fig. 8 Closed-loop pole locations of linear roll/yaw and pitch momentum removal scheme.

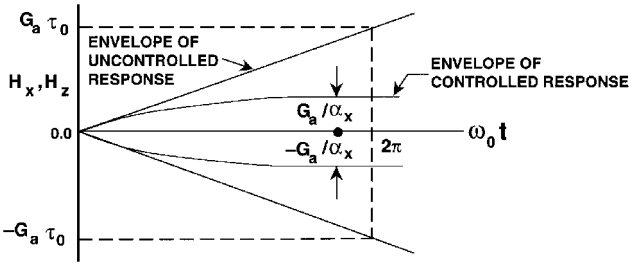

a) Roll/yaw momentum envelope

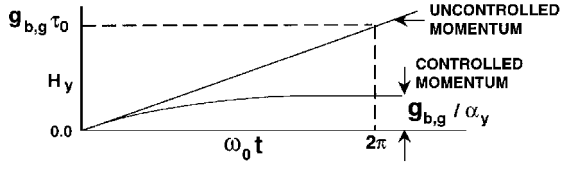

b) Pitch momentum response

Fig. 9 Uncontrolled and controlled momentum components under constant disturbances and magnetic control torque.

α_x and α_z, we impose the condition[16] that $H_{x,\mathrm{ss}} = H_{z,\mathrm{ss}}$, consistent with a cylindrical momentum envelope; this yields

$$\alpha_x = \alpha_z \tag{28}$$

$$H_{x,\mathrm{ss}} = |G_a|/\alpha_x = H_{z,\mathrm{ss}} \tag{29}$$

With $\alpha_x = \alpha_z$, the closed-loop poles of the roll/yaw momentum removal dynamics are found at $-\alpha_x \pm j\omega_0$ (see Fig. 8, $j^2 = -1$; also see Fig. 9). In terms of the undamped natural frequency ω_n and the damping coefficient ζ, α_x and ω_0 are

$$\alpha_x = \alpha_z = \zeta\omega_0/\sqrt{1-\zeta^2} \qquad \omega_0 = \omega_n\sqrt{1-\zeta^2} \tag{30}$$

One can now determine α_x by specifying a desirable damping coefficient ζ. Or, alternately, knowing $|G_a|$, a constant torque in the orbit plane, and the tolerable steady-state roll/yaw momentum amplitude $H_{x,\mathrm{ss}} = H_{z,\mathrm{ss}}$ according to the wheels' capacity, α_x can be determined from Eq. (29). The ratio between $H_{x,\mathrm{ss}}$ and the secular momentum $H_{x,\mathrm{sec}} \triangleq G_a\tau_0$ at the end of one orbit period τ_0 in the absence of a magnetic controller (see Fig. 9) is

$$H_{x,\mathrm{ss}}/H_{x,\mathrm{sec}} = \sqrt{1-\zeta^2}/2\pi\zeta \tag{31}$$

Thus, by specifying ζ, the preceding ratio is specified.

For the specification of the real pole $-\alpha_y$ for the pitch axis (Fig. 8), the steady-state pitch momentum $H_{y,\mathrm{ss}}$ is arrived at by integrating Eq. (27b) (see Fig. 9)

$$H_{y,\mathrm{ss}} = g_{b,g}/\alpha_y \tag{32}$$

Therefore, knowing the constant pitch torque and the tolerable $H_{y,\mathrm{ss}}$ consistent with the wheels' capacity, α_y is determined from Eq. (32). Alternately, since the secular pitch momentum $H_{y,\mathrm{sec}}$ accumulated in one orbit period due to the constant torque $g_{b,g}$ is $g_{b,g}\,\tau_0$, we may specify the following ratio instead:

$$H_{y,\mathrm{ss}}/H_{y,\mathrm{sec}} \triangleq 1/n_y = 1/(\alpha_y\tau_0) \tag{33}$$

Thus, α_y is specified by specifying the desired momentum ratio n_y.

Having determined α_x and α_y (and $\alpha_z = \alpha_x$), the gains g_1, g_2, and g_3 are arrived at by solving Eqs. (26):

$$g_1 = \tfrac{3}{8}\hat{\alpha}_x\sec^2\xi + \tfrac{1}{4}\hat{\alpha}_y\,\mathrm{cosec}^2\xi \tag{34a}$$

$$g_2 = \tfrac{5}{4}\hat{\alpha}_x\,\mathrm{cosec}^2\xi - \tfrac{1}{2}\hat{\alpha}_y\cos^2\xi/\sin^4\xi \tag{34b}$$

$$g_3 = -\tfrac{3}{2}\hat{\alpha}_x\sec^2\xi + \hat{\alpha}_y\,\mathrm{cosec}^2\xi \tag{34c}$$

where $\hat{\alpha}_i = \alpha_i/\kappa^2$ $(i = x, y, z)$ and $\hat{\alpha}_x = \hat{\alpha}_z$. The elegance of the technique is that the nettlesome problem of choosing weighting matrices, solving the Riccati equation,[3–8] etc., are all avoided, and the closed-loop momentum amplitude is specified according to the wheels' capacity, and that furnishes the required closed-loop poles forthwith.

Special Cases

For stability, each of the three gains must be positive, but for some orbit inclinations the pitch or yaw dipole gains could become negative because of the negative terms in Eqs. (34b) and (34c), violating the stability condition and causing unacceptable power consumption by the magnets. In that event, the spacecraft need not carry a pitch or yaw electromagnet. Two such cases are possible, as shown next.

Low-Inclination Orbits

When the orbit inclination angle i is small, the pitch dipole makes a small angle with the magnetic field. As a result, the negative term on the right-hand side of Eq. (34b) (recall that for untilted dipole model, $\xi = i$) becomes larger than the positive term. The gain g_2 then must be set to zero. This is well known because a pitch dipole is not used for the orbits near equator. But that renders Eqs. (34a) and (34c) invalid, and the original equations (26) must be then reverted to, arriving at

$$\hat{\alpha}_x = g_3\cos^2\xi \tag{35a}$$

$$\hat{\alpha}_y = \sin^2\xi(2g_1 + g_3/2) \tag{35b}$$

$$\hat{\alpha}_z = g_1\cos^2\xi \tag{35c}$$

Because there are only two gains g_1 and g_3, the three quantities $\hat{\alpha}_x$, $\hat{\alpha}_y$, and $\hat{\alpha}_z$ cannot be all specified independently. Hence, if we again impose the requirement $\hat{\alpha}_x = \hat{\alpha}_z$, Eqs. (35) lead to

$$g_1 = g_3 = \hat{\alpha}_z\sec^2\xi = \hat{\alpha}_x\sec^2\xi \tag{36}$$

Thus, both gains are now specified, rendering $\hat{\alpha}_y$ equal to

$$\hat{\alpha}_y = \tfrac{5}{2}\hat{\alpha}_x\tan^2\xi \tag{37}$$

equivalent to, according to Eqs. (30) and (33),

$$n_y = 5\pi\zeta\tan^2\xi/\sqrt{1-\zeta^2} \tag{38}$$

and thus n_y is also fixed.

High-Inclination Orbits

For such orbits, the negative term on the right-hand side of Eq. (34c) could be larger than the positive term, leading to a negative yaw gain, and therefore g_3 must be set to zero. The GPS satellites at $i = 63$ deg, for example, are not equipped with yaw electromagnets. For roll and pitch electromagnets and $g_3 = 0$, Eqs. (26) lead to

$$\hat{\alpha}_x = 2g_2\sin^2\xi \tag{39a}$$

$$\hat{\alpha}_y = 2g_1\sin^2\xi \tag{39b}$$

$$\hat{\alpha}_z = g_1\cos^2\xi + \tfrac{1}{2}g_2\sin^2\xi \tag{39c}$$

As before, imposing the condition $\hat{\alpha}_x = \hat{\alpha}_z$, we arrive at

$$g_1 = \tfrac{3}{2}g_2\tan^2\xi \tag{40}$$

The gain g_2 is determined by using Eq. (39a) and $\hat{\alpha}_y$ by using Eq. (39b), which then yield

$$n_y = 3\pi\zeta \tan^2 \xi / \sqrt{1-\zeta^2} \tag{41}$$

Thus, analogous to the low-inclination orbits, n_y cannot be specified independently.

Illustration

Figures 10 and 11 illustrate performance of the linear controller. Unlike the previous two illustrations, the cyclic thresholds about all three axes are now taken to be zero. Because of the low inclination, $i = 28.5$ deg, the pitch magnet gain g_2 given by Eq. (34b) turns out to be negative and, therefore, the alternate scheme [Eqs. (35–38)] is employed. The roll and yaw electromagnet gains are further simplified by using the untilted geomagnetic field model. Thus, for the damping coefficient $\zeta = 0.95$, $g_1 = g_3 \approx 1.35E7$, $n_y = 14.09$, $H_{x,ss}/H_{x,sec} = 0.0525$, and $H_{y,ss}/H_{y,sec} = 0.07$. For the spacecraft at hand, it is known that, for the so-called beta angle of the array equal to 45 deg, $G_a = 1.7E\text{-}4$ N · m and $g_{b,g} = 3.8E\text{-}5$ N · m. Therefore, the secular momentum buildup in one orbit is $H_{x,sec} = G_a\tau_0 = 1.18$ N · m · s and $H_{y,sec} = g_{b,g}\tau_0 = 0.26$ N · m · s. The predicted steady-state cyclic momentum amplitudes are, therefore, $H_{x,ss} = 0.062$ N · m · s and $H_{y,ss} = 0.018$ N · m · s. The actual steady-state amplitudes in Fig. 11 are larger because of cyclic disturbance torques in the inertial frame and because the magnetic field varies along the orbit and rotates with the Earth. The instantaneous roll and yaw electromagnets' strength, limited to 60 amp · m^2, is shown in Fig. 11. Comparing the power consumption data, we determine that the power consumed by the magnets is now 35% less than that for the bang-bang controller and nearly twice the amount used by the earlier linear magnetic controller. However, comparing the peak-to-peak wheel speed variations (not shown here due to space limitations), we still find that the bang-bang controller controls this variation within tighter bounds than the linear controller does.

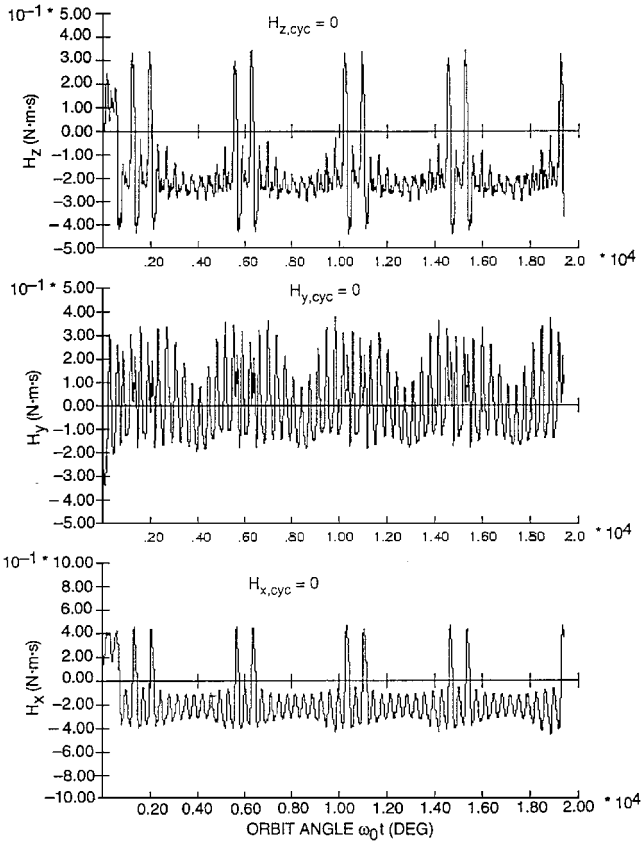

Fig. 10 Performance of the linear magnetic controller based on dynamic analysis: wheel momentum in orbit frame.

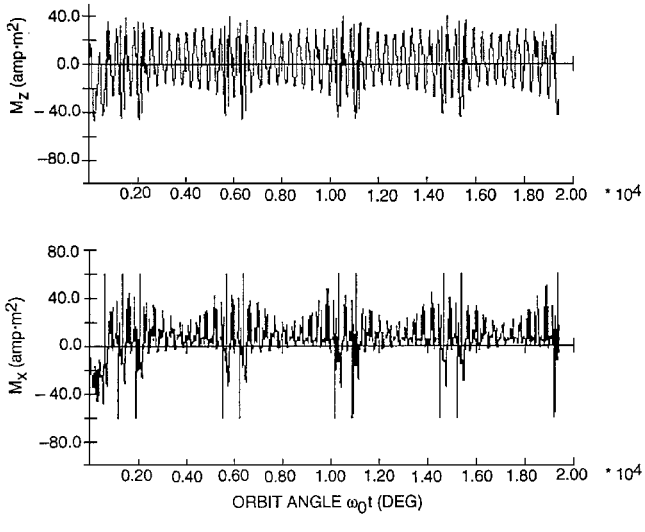

Fig. 11 Variation of the roll and yaw electromagnets strengths.

III. Concluding Remarks

Three magnetic momentum removal schemes are compared: 1) linear $\boldsymbol{H} \times \boldsymbol{B}$ law; 2) bang-bang $\boldsymbol{H} \times \boldsymbol{B}$ law, both based on the ratio of a constant disturbance torque with a constant, orbit-averaged magnetic control torque; and 3) a linear $\boldsymbol{H} \times \boldsymbol{B}$ law based on the classical closed-loop pole placement and desired roll/yaw and pitch steady-state momentum amplitudes. This last technique is developed. It is recommended for the following reasons.

1) The control gains for the roll, pitch and yaw electromagnets are determined methodically to meet the specified steady-state, tolerable wheel momenta under disturbances and magnetic control; this implicitly specifies the roll/yaw and pitch closed-loop pole locations in the frequency domain. The underlying relationships are developed in the paper.

2) If an electromagnet is not situated favorably relative to the orbit-averaged geomagnetic field (that is, if it cannot produce significant magnetic control torque), the scheme indicates so. Indeed, the illustrations bear out the known facts that for low-inclination spacecraft a pitch magnet is ineffective and for high-inclination spacecraft a yaw magnet is ineffective compared to the roll magnet.

3) The wheel speed varies over a small range because the environmental disturbances are counteracted essentially by the magnets, relieving the wheels to counteract more effectively the non-environmental disturbances.

4) The variation in the disturbance torque arising from a) changing orientation of the array relative to the spacecraft, b) alternate zero and π-rad yaw orientations of the spacecraft for sun tracking, and c) parametric changes in the inertia or optical properties over a spacecraft's operational lifetime are inconsequential, for the magnets will remove any undesirable wheel momentum and, therefore, the need for estimating a varying amplitude of a disturbance torque is obviated.

A continuous variation of the current through the electromagnets in the recommended scheme, as against a fixed current in a bang-bang scheme, may impose additional weight and cost. But the on-orbit software requirements to implement the recommended controller may be essentially the same as for the other schemes.

Acknowledgment

The extensive numerical results included in this paper were carefully generated by T. C. Witham. With great pleasure, I acknowledge his conscientious and painstaking efforts to simulate the control schemes analyzed here.

References

[1] Ross, C. H., and Worley, E., "Optimized Momentum and Attitude Control System (MACS) for Skylab," AIAA Paper 71-938, Aug. 1971.

[2] Powell, B. K., "Gravity Gradient Desturation of a Momentum Exchange Attitude Control System," AIAA Paper 71-940, Aug. 1971.

[3]Sunkel, J. W., and Shieh, L. S., "Optimal Momentum Management Controller for the Space Station," *Journal of Guidance, Control, and Dynamics*, Vol. 13, No. 4, 1990, pp. 659–668.

[4]Mapar, J., "Innovative Approach to the Momentum Management Control for Space Station Freedom," *Journal of Guidance, Control, and Dynamics*, Vol. 16, No. 1, 1993, pp. 175–181.

[5]Sunkel, J. W., Shieh, L. S., and Zhang, J. L., "Digital Redesign of an Optimal Momentum Management Controller for the Space Station," *Journal of Guidance, Control, and Dynamics*, Vol. 14, No. 4, 1991, pp. 712–723.

[6]Singh, H., and Naidu, D. S., "Regional Pole Placement for Momentum Management for the Space Station," *Proceedings of AIAA Guidance, Navigation, and Control Conference* (Scottsdale, AZ), AIAA, Washington, DC, 1994, pp. 647–652.

[7]Balas, G. J., Packard, A. K., and Harduvel, J. T., "Application of μ-Synthesis Techniques to Momentum Management and Attitude Control of the Space Station," *Proceedings of AIAA Guidance, Navigation, and Control Conference* (New Orleans, LA), AIAA, Washington, DC, 1991, pp. 565–575.

[8]Wie, B., Hu, A., and Singh, R., "Multibody Interaction Effects on Space Station Attitude Control and Momentum Management," *Journal of Guidance, Control, and Dynamics*, Vol. 13, No. 6, 1990, pp. 993–999.

[9]Kroncke, G. T., and Fuchs, R. P., "An Algorithm for Magnetically Dumping GPS Satellite Angular Momentum," *Journal of Guidance and Control*, Vol. 1, No. 4, 1978, pp. 269–272.

[10]Ferguson, J. R., and Kroncke, G. T., "Dumping Momentum Magnetically on GPS Satellites," *Journal of Guidance and Control*, Vol. 4, No. 1, 1981, pp. 87–90.

[11]Camillo, P. J., and Markley, F. L., "Orbit-Average Behavior of Magnetic Control Laws for Momentum Unloading," *Journal of Guidance and Control*, Vol. 3, No. 6, 1980, pp. 563–568.

[12]McLoughlin, F. A., and Tung, F. C., "Momentum Unloading Techniques for the Gamma Ray Observatory," AIAA Paper 84-1838, Aug. 1984.

[13]McElvain, R. J., "Satellite Angular Momentum Removal Utilizing the Earth's Magnetic Field," *Torques and Attitude Sensing in Earth Satellite*, edited by S. F. Singer, Academic, New York, 1964, pp. 137–158.

[14]Buckingham, A. G., and Braumiller, J., "The Application of an Electromagnetic Actuation System to the Momentum Desaturation of Space Station Control Moment Gyros," AIAA Paper 71-939, Aug. 1971.

[15]Carrington, C. K., Baracat, W. A., and Junkins, J. L., "A Comparative Study of Magnetic Momentum Dump Laws," AIAA Paper 81-139, Aug. 1981.

[16]Lebsock, K. L., "Magnetic Desaturation of a Momentum Bias System," *Journal of Guidance, Control, and Dynamics*, Vol. 6, No. 6, 1983, pp. 477–483.

[17]Hablani, H. B., "Sun-Tracking Commands and Rection Wheel Sizing with Configuration Optimization," *Journal of Guidance, Control, and Dynamics*, Vol. 17, No. 4, 1994, pp. 805–814.

[18]Hablani, H. B., "Magnetic Precession and Product-of-Inertia Nutation Damping of Bias Momentum Satellites," *Proceedings of the AIAA Guidance, Navigation, and Control Conference* (Scottsdale, AZ), AIAA, Washington, DC, 1994, pp. 154–169.

[19]Eller, T. J., and Wagie, D. A., "Earth's Magnetic Field Models for Dumping Momentum Magnetically on GPS Satellites," *Journal of Guidance, Control, and Dynamics*, Vol. 5, No. 5, 1982, pp. 438–441.

[20]Flashner, H., and Burns, T. F., "Spacecraft Momentum Unloading: The Cell Mapping Approach," *Journal of Guidance, Control, and Dynamics*, Vol. 13, No. 1, 1990, pp. 89–98.